

## Sliding-mode control of brushless dc motor\*

V. RAMANARAYANAN<sup>†</sup>, ASIF SABANOVIĆ<sup>‡</sup> and SLOBODAN ĆUK

Power Electronics Group, California Institute of Technology, Pasadena, CA 91125, USA.

### Abstract

Brushless dc motor (BLDC motor) is an attractive option for variable speed applications. It is more robust than the dc motor and the performance is comparable to the dc motor. Sliding mode control may be applied to the control of BLDC motor as presented in this paper.

**Key words:** Brushless dc motor, sliding mode control.

### 1. Introduction

Direct current motors had occupied a wide spectrum of applications for variable speed drives, because of their simplicity and versatility of control. The simplicity is obtained owing to the typical mechanical construction of the dc machine, and the brush orientation leading current into the armature enables orthogonality between the magnetomotive force (MMF) produced by the current and the main excitation MMF. As a result, for any given excitation to the dc machine, the armature voltage determines operating speed and the armature MMF determines the developed torque. Under constant excitation, the dc motor is essentially a linear system resulting in the simplicity of control.

On the other hand, the presence of commutator and brushes contribute to the wear and tear and the consequent maintenance overheads of the drive. These disadvantages have led to the application of ac machines, which are robust in construction, for variable speed applications<sup>1</sup>.

Polyphase synchronous and asynchronous motors operate at fixed speed (synchronous motors) or nearly fixed speed (asynchronous motors), when supplied from a constant frequency polyphase bus. They may be operated at variable speed when supplied from a variable frequency source. Conversion of power to polyphase variable frequency system became viable with high-speed solid-state switches, thus opening up the application of ac motors for variable speed applications. Different converter topologies such as voltage- and current-fed inverters, etc., are being used for the purpose. Different modulation

\* First presented at the Platinum Jubilee Conference on Systems and Signal Processing held at the Indian Institute of Science, Bangalore, India, during December 11–13, 1986.

<sup>†</sup> Present address: Department of Electrical Engineering, Indian Institute of Science, Bangalore 560 012.

<sup>‡</sup> Energoinvest-IRCA, Sarajevo, Yugoslavia.

techniques such as pulse width modulation (PWM), pulse amplitude modulation (PAM), etc., are used to control the amplitude of the output voltage and to minimise the harmonic content of the output polyphase power.

From the point of view of the motor being controlled, different mathematical descriptions (voltage-fed machine, stationary- and rotating-reference frames, etc.) exist giving rise to different control options such as current-fed and constant volts/hertz operations, etc. More recently the rotating-reference frame description of the machine and the vector control or the field-oriented control is being very successfully applied for superior dynamic performance of the ac drive<sup>2</sup>.

One common feature among all the above control methods is that there is a converter (switching power processor) with its characteristic control loop (phase control, quasi-square wave control, PWM, etc.) and dynamics; and there is a motor (synchronous or asynchronous) with its static and dynamic characteristics. The two are then combined together to develop an overall model. Suitable feedback techniques are then employed to achieve the control objectives such as speed and position controls.

In contrast to the above, the theory of variable structure systems and the concept of sliding mode control may be used on the power processor and the motor together to develop a control strategy that is integrated to the final control objective namely, speed and position controls, etc.

In this paper, application of sliding mode control to permanent magnet synchronous motor is presented. The overall drive is referred to as brushless dc motor (BLDC motor). Decoupled characteristics are obtained through field orientation. Linear control theory and sliding mode control are combined to develop a simple control strategy and feedback compensator. Bidirectional speed control and overload protection are featured.

Section 2.1 introduces the theory of variable structure systems and the concept of sliding mode control through the example of chopper-driven dc motor in a graphical manner through the phase plane. Such a presentation helps one appreciate the simplicity and strengths of sliding mode control. Besides, it also helps lay the ground work for understanding the control of BLDC motor, developed subsequently.

Section 2.2 brings out the unity behind the separately excited dc motor and the permanent magnet synchronous motor.

In the transformed rotating reference frame ( $d, q$  axes), the defining equations of the permanent magnet synchronous motor are essentially the same as the defining equations of the separately excited dc motor. The transformations between the three-phase stationary reference frame ( $A, B, C$ ) to two-phase stationary reference frame ( $\alpha, \beta$ ) and the two-phase stationary reference frame ( $\alpha, \beta$ ) to the two-phase synchronously rotating reference frame ( $d, q$ ) are given in Section 2.3.

Section 2.4 applies the same control strategy as developed for the dc motor to the BLDC motor. The control method is interpreted in a graphical manner to develop the polyphase switching decisions.

The simplest of the control methods, namely, current-controlled BLDC motor is given in Section 2.5. Simple extension to speed control is also indicated. Section 2.6 describes the strategy of sliding-mode speed controller.

Section 3 deals with the practical considerations and the hardware realization of the various control schemes. The hardware realization of the current-controlled BLDC motor is given in Section 3.1 along with experimental results.

In practice, direct sliding-mode control as developed in Section 2.6 requires access to the speed derivative. Estimation of speed derivative calls for high quality tachogenerators or high resolution position sensors and is not always economical. An indirect or modified sliding-mode control strategy is developed in Section 3.2 using the motor speed and current as the feedback variables. A design criterion is evolved and the hardware realization is presented. Experimental results verifying the design procedure are presented.

Practical realization of the control scheme requires the generation of the currents in the transformed coordinates. With digital circuit blocks it is done quite inexpensively. However, for certain applications these transformations may be done approximately, leading to further savings in hardware, without perceptible difference in performance. Section 3.3 deals with these practical aspects.

## 2. Theory

### 2.1 Variable structure systems and sliding-mode control

Variable structure systems are characterized by a time variant topology. As a result the control action is discontinuous and the plant nonlinear. The theory of variable structure systems and sliding-mode control form a pair of mutually complementary analysis and design tools<sup>3</sup>. What follows is an introduction of these concepts through the example of a chopper-driven dc motor.

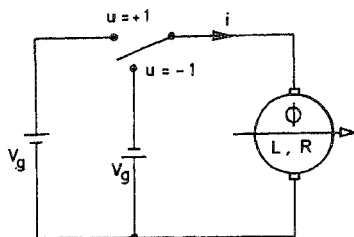
Figure 1 shows the chopper-driven dc motor. The defining equations of the system for constant excitation are given by

$$L(di/dt) + Ri + K_E\omega = V_g u \quad (2.1.01)$$

$$J(d\omega/dt) + B\omega + T_L = K_T i \quad (2.1.02)$$

where

$L$	= armature inductance;	$R$	= armature resistance;
$K_E$	= back emf constant;	$\omega$	= speed of rotor
$T_L$	= load torque;	$K_T$	= torque constant;
$i$	= armature current;	$V_g$	= source voltage;
$J$	= moment of inertia;	$B$	= friction coefficient;
$u$	= discontinuous control, $\pm 1$ ;	$\phi$	= air gap flux.



$$L \frac{di}{dt} + Ri + K_E \omega = V_g u; \quad J \frac{d\omega}{dt} + B\omega + T_L = K_T i.$$

FIG. 1. Chopper-driven dc motor — definition of terms and the defining equations under constant excitation.

The above description is valid at all times. The control input  $u$  is the only discontinuous variable and takes on the value of either  $+1$  or  $-1$ , depending on the switch position as shown in fig. 1. After some manipulation the system eqns (2.1.01) and (2.1.02) may be put in the following form:

$$X = A^*X + B^*u + T^* \quad (2.1.03)$$

where

$$A^* = \begin{bmatrix} 0 & 1 \\ -(K_T K_E / JL) \{1 + (BR / K_T K_E)\} & -\{(R/L) + (B/J)\} \end{bmatrix}; \quad B^* = \begin{bmatrix} 0 \\ (K_T V_g / JL) \end{bmatrix}$$

$$X = \begin{bmatrix} \omega - \omega^* \\ \frac{d(\omega - \omega^*)}{dt} \end{bmatrix}; \quad T^* = \begin{bmatrix} 0 \\ \frac{-R(T_L + B\omega^*) - K_T K_E \omega^*}{JL} \end{bmatrix}$$

and  $\omega^*$  is the desired speed. The system states have been assigned as the output speed error and its derivative, so that the desired operating point is given by the state vector  $X = 0$ . The control problem now reduces to establishing a switching strategy to select an appropriate  $u$  at any instant of time to meet the dynamic requirements of the system.

Suppose that it is desired to achieve a response of zero steady-state error and a stable first order transient response with a time constant of  $\tau$ . These requirements may be expressed as the following differential equation:

$$(\omega - \omega^*) + \tau \frac{d(\omega - \omega^*)}{dt} = 0. \quad (2.1.04)$$

Equation (2.1.04) may be represented in matrix form as

$$\sigma = GX = 0; G = [1 \ \tau] \quad (2.1.05)$$

in which  $\sigma$  is a weighted sum of the states of the system and  $\sigma = 0$  may be visualized to represent a line in the two-dimensional space, whose axes are the states of the system.

The principle of sliding-mode control is to constrain the system, by suitable control strategy, to operate such that eqn (2.1.05) is satisfied. These ideas may be best understood by considering the phase plane of the system to obtain a graphical interpretation of the sliding-mode control<sup>4</sup>.

Figure 2 shows the phase plane of the chopper-driven dc motor. The system states are the output speed error  $(\omega - \omega^*)$  and the angular acceleration  $(d\omega/dt)$ . The instantaneous state of the system is represented on the phase plane by a point, whose coordinates are the output speed error and the angular acceleration at that instant. If the instantaneous

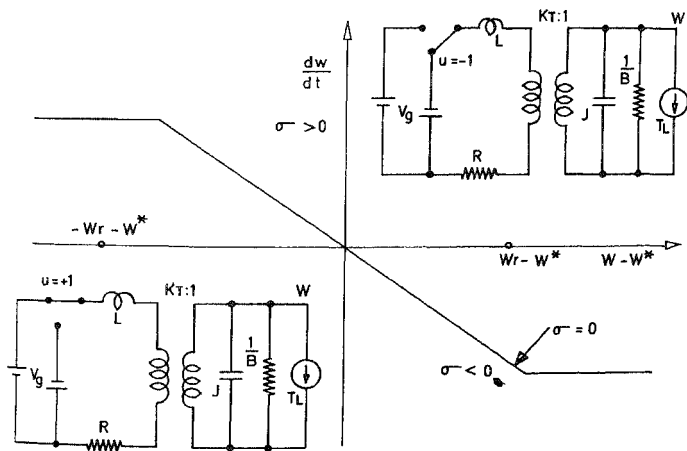


FIG. 2. Chopper-driven dc motor in the phase plane. The sliding line  $\sigma = 0$  partitions the phase plane into two regions ( $\sigma < 0$  and  $\sigma > 0$ ). The control and motor equivalent circuit in each region is shown. The steady-state operating points for each control inputs ( $\omega_r - \omega^*$  for  $u = +1$  and  $-\omega_r - \omega^*$  for  $u = -1$ ) are also shown. The control strategy is  $u = +1$  for  $\sigma < 0$  and  $u = -1$  for  $\sigma > 0$ .

state of the system is known, the switch position at that instant ( $u$ ) and the input voltage ( $V_g$ ) uniquely determine the future evolution of the system states for the duration of that switch position. Under steady state, the output speed error is zero and so is the angular acceleration. The desired steady-state operating point is therefore the origin in the phase plane. The line shown as  $\sigma = 0$  (sliding line) partitions the phase plane through the origin into two regions ( $\sigma > 0$  and  $\sigma < 0$ ). The special shape of the sliding line away from the origin is explained later.

The control inputs, namely, the switch position and the applicable equivalent circuits, are also shown in fig. 2, corresponding to the two regions of the phase plane.

If the armature is excited by  $+V_g$  ( $u=1$ ), then the steady-state speed of the motor would be  $\omega_r$ . This steady-state operating point for  $u = +1$ , is shown on the positive  $X$  axis as  $(\omega_r - \omega^*)$ . Similarly if the armature is excited by  $-V_g$  ( $u = -1$ ), then the steady-state speed of the motor would be  $-\omega_r$ . This steady-state operating point for  $u = -1$ , is shown on the negative  $X$  axis as  $(-\omega_r - \omega^*)$ . When no control is exercised, the steady-state operating points for the two different switch positions ( $u = +1$ , and  $u = -1$ ) are located in the opposite regions ( $\sigma < 0$  and  $\sigma > 0$ ) of the phase plane. As a result any switching action causes the system state to move towards the sliding line and cross into the other region. When the switching strategy shown in fig. 2 ( $u = +1$  for  $\sigma < 0$  and  $u = -1$  for  $\sigma > 0$ ) is implemented, the system state moves toward the sliding line and, having hit the sliding line is constrained to remain in the neighbourhood of the sliding line owing to the switching action. On the sliding line the only steady-state operating point is the origin. At all other points on the sliding line, a gradient exists which forces the operating point to move towards the origin. Therefore once the system state reaches the sliding line, the switching action ( $u = \pm 1$ ) forces the system-state to slide along the sliding line and reach the desired steady state operating point, namely the origin ( $\omega = \omega^*$ ). Despite the terminology 'sliding line', it is the system state that does the sliding along the line. Since the system is constrained to be on the sliding line at all times, the response is decided by the chosen sliding line and not by the motor parameters. Notice that the switching frequency is not constant as in the case of a conventional chopper. The switching is free running with the only objective of maintaining the system state to remain in the neighbourhood of the sliding line. The static and dynamic response of the system is therefore dependent only on the sliding line chosen and not on the motor parameters. For example, for the chosen sliding line given by eqn (2.1.04), the steady-state response is

$$\omega = \omega^*, \quad (2.1.06)$$

and the dynamic response is

$$\omega = \omega^* (1 - e^{-t/\tau}). \quad (2.1.07)$$

The dynamic response of the overall system (chopper and motor together) is a function of the chosen sliding line only. In contrast, in the case of a conventional chopper, dynamic models of the chopper and the motor have to be considered to develop a suitable control strategy. Even then, any feedback compensator designed will not be totally insensitive to

the motor parameters. This property of insensitivity to plant parameters is the main characteristics of sliding-mode control in contrast to conventional linear control.

It may be seen that the sliding line is shaped such that the system states are limited along the vertical axis. These limits on the acceleration (vertical axis) serve the useful purpose of protecting the motor against overcurrent, since the acceleration at any instant is directly related to the current drawn by the motor. The horizontal sections of the sliding line signify the current limited region of operation and the central portion of the sliding line passing through the origin signifies the speed-controlled region of operation.

In order to be able to directly extend this concept of control later on to BLDC motor, it is worthwhile to understand the switching decision ( $u = +1$  or  $u = -1$ ) qualitatively. This is necessary because the switching converter for driving the polyphase motor has three pairs of switches corresponding to the three phases of the motor. Accordingly, at any instant, three switch positions are to be determined. To enable this the switch inputs may be qualitatively stated as 'accelerate' ( $u = +1$ ) and 'decelerate' ( $u = -1$ ). Later on these qualitative switch input commands 'accelerate' and 'decelerate' will be related through a look-up table to the three-phase switch inputs, when applied to the BLDC motor control.

## 2.2 Separately excited dc motor and synchronous motor

Figure 3a shows the construction of the separately excited dc motor in its simplest form. The field winding on the stator produces a fixed magnetic field in the air gap. The dc current fed through the commutator into the armature produces an armature MMF fixed in space independent of the position of the rotor, though the current in any conductor in the armature is alternating. The field MMF and the armature MMF are stationary in space and orthogonal to each other.

Figure 3b shows the construction of a three-phase synchronous motor in its simplest form. Direct current fed into the field winding on the rotor produces a field MMF which is rotating in the airspace of the motor owing to the rotation of the rotor. Three-phase balanced currents into the three-phase armature winding produces an armature MMF rotating at synchronous speed. The field MMF and the armature MMF are both rotating at synchronous speed and so stationary relative to each other. Useful torque is produced when the rotor is rotating at synchronous speed and the field MMF and armature MMF are not coincident. This explains the lack of average torque in a synchronous motor at any speed other than synchronous speed. Further, for maximum torque, the field MMF and the armature MMF must be orthogonal to each other.

The dc motor may be considered as an inverter-fed, inside-out synchronous motor. Direct current in the field winding produces a stationary field MMF. The commutator may be thought of as a shaft position dependent inverter which converts the dc input current to an ac current of the right frequency so that the rotating MMF produced by the ac current in the rotating armature conductors is stationary with respect to the field MMF at all speeds. The commutator ensures that the armature current is at synchronous frequency at all speeds. The brush orientation ensures the orthogonal phase relationship

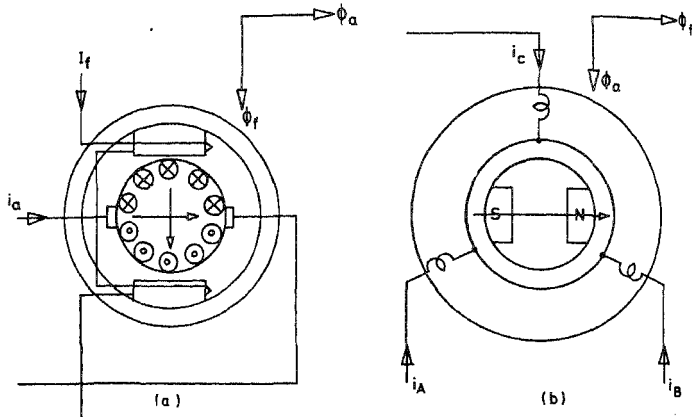


FIG. 3. The construction of dc motor and synchronous motor. (a) Direct current motor: The field winding on stator produces a stationary field. The armature winding on the rotor is fed through the commutator. The armature MMF is stationary in space and orthogonal to the field MMF. (b) Synchronous motor: For simplicity the field winding carrying a dc current is shown as a pole pair on the rotor. The rotor MMF is rotating in space at the rotational speed of the shaft. Armature winding on stator fed by three-phase power produces an MMF in space rotating at synchronous frequency. When shaft speed equals the synchronous speed the stator MMF and the rotor MMF are stationary relative to each other.

between the armature MMF and the field MMF. As a result useful maximum torque is produced at all operating speeds.

In order to obtain an equivalent dc motor operation from a synchronous motor, it is necessary to feed dc power to the three-phase windings of the synchronous motor stator through an electronic commutator (power converter). The frequency and phase relationship of the stator currents must be synchronized to the rotor position so that orthogonality between armature MMF and rotor MMF is obtained at all speeds. For this reason BLDC motor is also referred to as electronically commutated motor (ECM).

As mentioned above, the field MMF and the armature MMF are both rotating in the airspace of the motor and are stationary with respect to each other. By proper phase relationship, the armature MMF and the field MMF are also made orthogonal to each other. This leads to the selection of a synchronously rotating reference frame in which the synchronous motor may be transformed to an equivalent dc motor. These transformations leading to the equivalent dc motor are introduced in Section 2.3.

### 2.3 $ABC-\alpha\beta-dq$ transformations

In this section the transformations on the permanent magnet-synchronous motor leading to the rotating reference frame equivalent dc motor description are laid out step by step.

One of the popular methods is to define the transformations mathematically, substitute them in the original equations to arrive at the desired results. But we follow the method of physically interpreting the transformations at every step, writing down the circuit equations directly in each reference frame, and relating the description in different reference frames with each other using some physical criterion. The reason to follow this method is that the mathematical transformations are firmly anchored to physical interpretations and the inter-relationship between the physical constants of the machine in different frames of reference is more readily apparent.

Figure 4 shows the essential construction of the permanent magnet-synchronous motor. The physical structure of the rotor is represented by the innermost circle. The rotor carries the permanent magnets providing constant field excitation. The rotor MMF in the absence of stator currents sets up an airgap flux of  $\phi_d$ . The outermost annular ring in fig. 4 represents the physical structure of the stator. The stator phase windings A, B and C are shown schematically to coincide with the direction in which the respective MMFs are oriented. The intermediate annular rings in fig. 4 represent fictitious structures which are helpful in stepping through the various transformations and are explained as we go along.

The defining equations of the machine are in three parts. First is the electrical subsystem definition relating the electrical quantities of the machine. The definition of the electrical subsystem depends on the chosen frame of reference. The second part is the

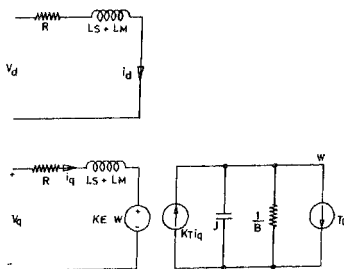
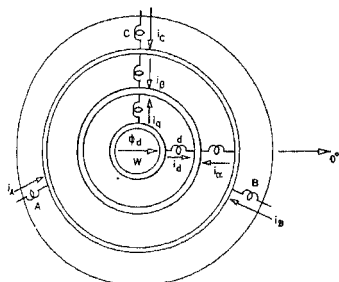


FIG. 4. A, B, C to  $\alpha, \beta$  to  $d, q$  transformations. The outermost annular ring and the innermost circle represent the physical stator and the rotor respectively. The second annular ring from outside represents a fictitious equivalent two-phase stator which when excited by appropriate two-phase currents would result in the same machine performance. The third annular ring from outside represents a fictitious two-phase equivalent 'rotor' which carrying dc currents ( $i_d$  and  $i_q$ ) results in the same performance as the original machine.

FIG. 5. The electrical equivalent circuit of the permanent magnet synchronous machine in the synchronously rotating ( $d, q$ ) reference frame. The voltages ( $v_d, v_q$ ) and the currents ( $i_d, i_q$ ) are dc quantities.

electromagnetic subsystem of the machine indicating the mechanism of torque generation. The electrical quantities in the torque relationship again depend on the chosen frame of reference. The last part is the mechanical subsystem relating the break up of the generated torque into load, friction and inertia. The selection of a frame of reference is to simplify the definition of the electrical subsystem and does not change the definition of the mechanical subsystem.

The definition of the mechanical subsystem is independent of the frame of reference and is given by

$$J(d\omega/dt) + B\omega + T_L = T_g \quad (2.3.01)$$

where the quantities  $J$ ,  $B$ ,  $T_L$  and  $\omega$  are as defined earlier in Section 2.1 and  $T_g$  is the generated torque.

The electrical subsystem equations are dependent on the frame of reference. In the physical stationary reference frame (stator represented by the outer-most circle and the rotor represented by the inner-most circle in fig. 4), the stator electrical circuit equations may be written from first principles as follows:

$$R_A i_A + L_{AA}(di_A/dt) + L_{AB}(di_B/dt) + L_{AC}(di_C/dt) + (d\psi_{Ad}/dt) = v_A \quad (2.3.02a)$$

$$L_{BA}(di_A/dt) + R_B i_B + L_{BB}(di_B/dt) + L_{BC}(di_C/dt) + (d\psi_{Bd}/dt) = v_B \quad (2.3.02b)$$

$$L_{CA}(di_A/dt) + L_{CB}(di_B/dt) + R_C i_C + L_{CC}(di_C/dt) + (d\psi_{Cd}/dt) = v_C \quad (2.3.02c)$$

where

$L_{XX}$  = self inductance of phase windings;

$R_X$  = resistance of phase windings;

$L_{XY}$  = mutual inductance between windings  $X$  and  $Y$ ;

$\psi_{Xd}$  = flux linkage to winding  $X$  due to rotor flux  $\phi_d$ ;

$v_X$  = phase voltage;  $i_X$  = phase current.

Under the assumptions of symmetrical balanced three-phase windings, without neutral conductor and sinusoidal flux distribution,

$$R_A = R_B = R_C = R; \quad L_{AA} = L_{BB} = L_{CC} = L_S;$$

$$L_{AB} = L_{BA} = L_{BC} = L_{CB} = L_{CA} = L_{AC} = -L_M;$$

$$i_A + i_B + i_C = 0.$$

Notice that  $L_{XY}$  is defined with a negative coefficient owing to the selection of positive current directions in fig. 4. Equations (2.3.02) may then be simplified as

$$Ri_A + (L_S + L_M)(di_A/dt) + (d\psi_{Ad}/dt) = v_A; \quad (2.3.03a)$$

$$Ri_B + (L_S + L_M)(di_B/dt) + (d\psi_{Bd}/dt) = v_B; \quad (2.3.03b)$$

$$Ri_C + (L_S + L_M)(di_C/dt) + (d\psi_{Cd}/dt) = v_C. \quad (2.3.03c)$$

The generated torque is the sum of the torques owing to the interaction between the rotor MMF and each of the stator-phase current MMFs. The generated torque due to each of the stator-phase currents depends on the rotor position. The total torque is given by

$$T_g = K \phi_d [i_A \sin(330^\circ + \omega t) + i_B \sin(210^\circ + \omega t) + i_C \sin(90^\circ + \omega t)] \quad (2.3.04)$$

where  $K$  is a proportionality constant with proper dimensions and  $\omega t$  is the instantaneous angular position of the rotor. Equation (2.3.04) may be further simplified as

$$T_g = K \phi_d \{(-i_A/2 - i_B/2 + i_C) \cos \omega t + (\sqrt{3}i_A/2 - \sqrt{3}i_B/2) \sin \omega t\}. \quad (2.3.05)$$

In eqn (2.3.03) the rotor position is implicit through the terms  $\psi_{Xd}$ . In eqn (2.3.05) the rotor position is explicit. Equations (2.3.03) and (2.3.05), define the electrical and the electromagnetic subsystems in the physical stator reference frame. The electrical quantities appearing in these equations are the same as what can be measured in the stator circuit.

The currents in the stator-phase windings of the motor produce an MMF in the active plane of the motor, which interacting with the rotor MMF in the same plane produces the required torque. This stator MMF may very well be produced by an equivalent stator with two-phase orthogonal windings carrying two-phase ac currents. The first step in simplifying the system equations is to transform the stationary reference frame three-phase stator equations (eqns (2.3.03) and (2.3.05)) to an equivalent stationary reference frame two-phase stator equations.

The second annular ring from outside in fig. 4 represents this fictitious stator with two-phase windings on it ( $\alpha$  and  $\beta$ ) as shown. Again from first principles the circuit equations and torque equation may be written down as below:

$$R^* i_\alpha + L^* (di_\alpha/dt) + (d\psi_{\alpha d}/dt) = v_\alpha; \quad (2.3.06a)$$

$$R^* i_\beta + L^* (di_\beta/dt) + (d\psi_{\beta d}/dt) = v_\beta; \quad (2.3.06b)$$

$$T_g = K \phi_d (i_\beta \cos \omega t - i_\alpha \sin \omega t). \quad (2.3.07)$$

The subscripted quantities represent the fictitious two-phase stator electrical quantities. The machine constants in the equivalent fictitious two-phase system are shown with asterisks. Their relationship to the original machine constants are yet to be established.

The next step is to find the relationship between the  $A, B, C$  system and the  $\alpha, \beta$  system. To do this we invoke the condition that the torques developed in the two systems are equal. Comparing eqn (2.3.05) and (2.3.07), we get

$$i_\alpha = -\sqrt{3} i_A/2 + \sqrt{3} i_B/2; \quad (2.3.08a)$$

$$i_\beta = -i_A/2 - i_B/2 + i_C. \quad (2.3.08b)$$

From eqns (2.3.08) and (2.3.03), we get

$$R^* = R; L^* = L_S + L_M; \quad (2.3.09a,b)$$

$$v_\alpha = -\sqrt{3}v_A/2 + \sqrt{3}v_B/2; \quad (2.3.10a)$$

$$v_\beta = -v_A/2 - v_B/2 + v_C; \quad (2.3.10b)$$

$$\psi_{\alpha d} = -\sqrt{3}\psi_{Ad}/2 + \sqrt{3}\psi_{Bd}/2; \quad (2.3.11a)$$

$$\psi_{\beta d} = -\psi_{Ad}/2 - \psi_{Bd}/2 + \psi_{Cd}. \quad (2.3.11b)$$

The system of equations in the two-phase stationary reference frame ( $\alpha, \beta$  axes) may be written as

$$Ri_\alpha + (L_S + L_M)(di_\alpha/dt) + (d\psi_{\alpha d}/dt) = v_\alpha; \quad (2.3.12a)$$

$$Ri_\beta + (L_S + L_M)(di_\beta/dt) + (d\psi_{\beta d}/dt) = v_\beta; \quad (2.3.12b)$$

$$T_R = K\phi_d(i_\beta \cos \omega t - i_\alpha \sin \omega t). \quad (2.3.13)$$

The system equations are still functions of rotor position. Just as before, the rotor position is implicit in eqns (2.3.12) and explicit in eqn (2.3.13). The electrical quantities appearing in eqns (2.3.12) and (2.3.13) are fictitious in the sense that they are not accessible at any point in the actual machine.

Polyphase currents in the stator at synchronous frequency produce an MMF rotating in the machine airspace in synchronism with the rotor MMF. The interaction between these stator and rotor MMFs produce the required torque. The rotating stator MMF may very well be produced by an equivalent set of windings rotating in space at synchronous speed but carrying dc currents. The next step in simplifying the system equations is to transform the system eqns (2.3.12) and (2.3.13) in the two-phase stationary reference frame into a two-phase frame of reference rotating in space at synchronous frequency.

The third annular ring from outside in fig. 4 represents this fictitious rotating structure carrying dc currents ( $i_d$  and  $i_q$ ) in the two-phase windings ( $d$  and  $q$  windings). The electrical circuit equations and the torque equation may be directly written as

$$R^* i_d + L^* (di_d/dt) + K_d \omega = v_d; \quad (2.3.14a)$$

$$R^* i_q + L^* (di_q/dt) + K_q \omega = v_q; \quad (2.3.14b)$$

$$T_q = -K \phi_d i_q. \quad (2.3.15)$$

Apart from resistive and inductive drops, the phase windings also have speed voltage term because the  $d, q$  windings are rotating in space. The machine parameters are shown with asterisks because their relationship to the original machine parameters is yet to be established. We now invoke the condition that the MMF produced by the  $d, q$  windings is the same as that produced by the windings and the generated torque in both the systems is equal. Comparing eqns (2.3.15) and (2.3.13), we get

$$i_q = i_\alpha \sin \omega t - i_\beta \cos \omega t. \quad (2.3.16)$$

Equating  $d$  axis MMF, we get

$$i_d = -i_\alpha \cos \omega t - i_\beta \sin \omega t. \quad (2.3.17)$$

From eqns (2.3.16) and (2.3.17), the inverse relationship is also obtained.

$$i_a = -i_d \cos \omega t + i_q \sin \omega t; \quad (2.3.18a)$$

$$i_\beta = -i_d \sin \omega t - i_q \cos \omega t. \quad (2.3.18b)$$

Further, assumption of sinusoidal flux distribution leads to

$$\psi_{\alpha d} = -\psi_d \cos \omega t; \quad (2.3.19a)$$

$$\psi_{\beta d} = -\psi_d \sin \omega t; \quad (2.3.19b)$$

where  $\psi_d$  is the maximum flux linkage due to rotor flux to stator ( $\alpha$ ,  $\beta$ ) windings. Substitution of eqns (2.3.18) and (2.3.19) into eqns (2.3.12) and (2.3.13) leads to

$$Ri_d + (L_S + L_M)(di_d/dt) - (L_S + L_M)i_q\omega = v_d; \quad (2.3.20a)$$

$$Ri_q + (L_S + L_M)(di_q/dt) + (L_S + L_M)i_d\omega + \psi_d\omega = v_q; \quad (2.3.20b)$$

$$T_g = -K\phi_d i_q. \quad (2.3.21)$$

Equations (2.3.20) and (2.3.21) describe the system in synchronously rotating frame of reference. As expected the electrical quantities in eqns (2.3.20) and (2.3.21) are all dc quantities. They are independent of rotor position. Again the electrical quantities expressed in eqns (2.3.20) and (2.3.21) are fictitious in the sense that they are not directly accessible at any point in the machine.

In the case of permanent magnet-synchronous motor the effective airgap between the rotor and stator is large, on account of the fact that the relative permeability ( $\mu_r$ ) of the permanent magnet material is nearly unity. As a result the cross-coupling terms in eqn (2.3.20) are negligible leading to the following approximation.

$$v_d \approx Ri_d + (L_S + L_M)(di_d/dt); \quad (2.3.22a)$$

$$v_q \approx Ri_q + (L_S + L_M)(di_q/dt) + K_E\omega; \quad (2.3.22b)$$

$$T_g = K_T i_q. \quad (2.3.23)$$

The constants  $\psi_d$  and  $-K\phi_d$  have been replaced in the eqns (2.3.22) and (2.3.23) by the more familiar back emf constant  $K_E$  and the torque constant  $K_T$ . The system of eqns (2.3.01), (2.3.22) and (2.3.23) may be more conveniently represented by the equivalent circuit shown in fig. 5

#### 2.4 Control strategy

In this section the converter topology and the switching strategy are explained. First current-controlled operation of the BLDC motor is developed. Speed regulation under sliding mode control is explained in a subsequent section.

The power circuit of the BLDC motor is shown in fig. 6. For a given motor armature current, maximum torque is generated when the armature MMF is orthogonal to the field MMF. Therefore the principle of control of BLDC motor is to maintain the stator MMF

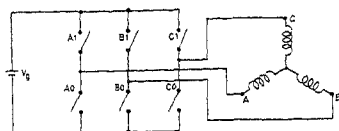


FIG. 6. Power circuit of the BLDC motor. The switches are synchronised to the rotor position and are the electronic counterpart of the mechanical commutator in a dc motor.

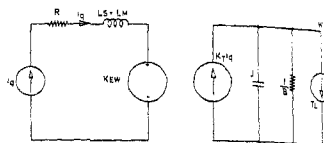


FIG. 7. Equivalent circuit of the current-controlled BLDC motor (with  $i_d = 0$ ). The mechanical system consisting of inertia ( $J$ ), friction ( $B$ ), and the load torque ( $T_L$ ) is represented by their electrical analog.

orthogonal to the rotor MMF, and of sufficient magnitude to support the load torque. This requirement translates in the rotating two-phase frame of reference ( $d$ - $q$  axes) into  $i_d$  being maintained at zero (for orthogonality between stator MMF and rotor MMF), and  $i_q$  maintained at the desired polarity and magnitude to produce the desired torque. Under these conditions the  $d$  axis part of the equivalent circuit given in fig. 5 vanishes and the overall system reduces to current-controlled dc motor as shown in fig. 7.

Next we relate the above requirements on  $i_d$  and  $i_q$  to a physical switching strategy. Figure 8 shows the active plane of the machine when the rotor is at position  $15^\circ$ . The orientation of the  $d$  axis coincides with the rotor MMF direction. The directed arrows represent the direction of the steady-state stator MMFs for the different switch positions shown alongside. For example, switch inputs ( $A_1, B_1, C_0$ ) produce a steady-state MMF vertically upwards. In the range of rotor position ( $0 < \omega t < 60^\circ$ ) this condition is equivalent to a positive dc current  $i_d$  and a positive dc current  $i_q$  of appropriate magnitude in the fictitious  $d$ - $q$  windings. Table I shows the interpretation of steady-state MMFs in terms of  $i_d$  and  $i_q$  and the validity of this interpretation in terms of the rotor position  $\omega t$ .

**Table I**  
Steady-state MMF along  $d$  and  $q$  axes

Switch position	Direction of MMF		Range of $\omega t$
	$d$ axis	$q$ axis	
$A_1, B_1, C_0$	$+I_d$	$+I_q$	$0^\circ < \omega t < 60^\circ$
$A_0, B_1, C_0$	$-I_d$	$+I_q$	$0^\circ < \omega t < 60^\circ$
$A_0, B_1, C_1$	$-I_d$	$-I_q$	$-30^\circ < \omega t < +30^\circ$
$A_0, B_0, C_1$	$-I_d$	$-I_q$	$0^\circ < \omega t < 60^\circ$
$A_1, B_0, C_1$	$+I_d$	$-I_q$	$0^\circ < \omega t < 60^\circ$
$A_1, B_0, C_0$	$+I_d$	$+I_q$	$-30^\circ < \omega t < +30^\circ$

Steady-state stator MMFs for different switching inputs and their interpretation in the synchronously rotating ( $d, q$ ) reference frame.

As we are interpreting a stationary quantity (steady-state stator MMF) in a rotating reference frame the interpretation is valid only in a limited range of rotor position. The last column indicates this limitation.

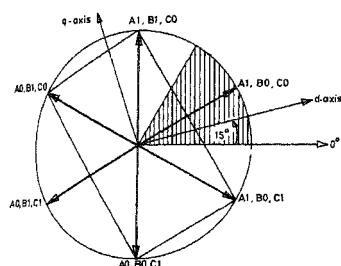


FIG. 8. Steady-state armature MMF for the various inverter switch positions. The directed arrows show the steady-state armature MMF in the active plane of the motor for the six possible switch inputs. The orientation of the  $d$ ,  $q$  axes are shown frozen in space corresponding to the rotor MMF at  $\omega t = 15^\circ$ .

As stated earlier we need to relate the requirements of  $i_d$  and  $i_q$  to the three-switch positions at any instant. There are two variables ( $i_d$  and  $i_q$ ) to be controlled with three-switch inputs indicating an extra degree of freedom. This extra choice available is also seen in Table I. However, we may select a set of control inputs which have a

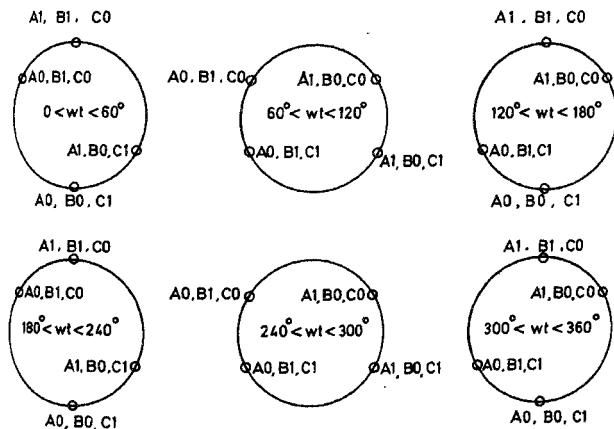


FIG. 9. Sufficient control inputs for each  $60^\circ$  wide sectors of the rotor position. The requirement of having to control independently only two quantities  $i_d$  and  $i_q$  with three independent switches ( $A$ ,  $B$ ,  $C$ ) results in the availability of more than sufficient control options. Notice that only four switch inputs of all the possible switch inputs are used in each sector.

consistent range of  $\omega t$ . These are  $(A_1, B_1, C_0)$ ,  $(A_0, B_1, C_0)$ ,  $(A_0, B_0, C_1)$  and  $(A_1, B_0, C_1)$  in the range of rotor positions ( $0 < \omega t < 60^\circ$ ). Figure 9 shows the set of switch inputs used for the control in each of the six different  $60^\circ$  wide sectors.

The method of control is to determine the error in the instantaneous value of the currents  $i_d$  and  $i_q$  and to select the appropriate switch inputs  $(A, B, C)$  in order to correct the error. The strategies for current-controlled BLDC motor and the speed-controlled BLDC motor are given in the subsequent sections.

### 2.5 Current-controlled BLDC motor

Constant current control is the simplest of the control methods. In each of the six sectors shown above in fig. 9 the instantaneous value of  $i_d$  and  $i_q$  enables one to select an appropriate power circuit switch position. For example, in the sector ( $0 < \omega t < 60^\circ$ ), if the value of  $i_d$  and  $i_q$  are higher than their desired values, the converter is switched to  $(A_0, B_0, C_1)$ , and so on. Rotor position and phase currents of the motor are sensed. By using the transformations given in Section 2.3, they are converted into  $i_d$  and  $i_q$ .  $i_d$  is checked against zero.  $i_q$  is checked against the desired value  $I_q^*$ . From these inputs and the sector in which the rotor MMF lies at any instant, the power circuit switch inputs are selected. Table II is a look-up table for this purpose.

The control scheme outlined above achieves regulation of the  $d$  axis and  $q$  axis currents. For proper BLDC motor operation, the  $d$  axis current  $i_d$  is maintained zero and the  $q$  axis current  $i_q$  is regulated to be equal to  $I_q^*$ . The current-controlled BLDC motor then may be represented by the block diagram shown in fig. 10. The quadrature axis current  $i_q$  and the speed  $\omega$  are both continuous signals. The shaft speed is related to the quadrature axis current  $i_q$  by first order dynamics. Simple linear feedback compensators may be used to realize an overall speed regulator scheme. However, what we follow in the subsequent sections is an alternative approach of sliding-mode speed regulation.

### 2.6 Sliding-mode speed controller

The BLDC motor drive may be represented by front-end converter and the rotating reference frame equivalent circuit of the motor as shown in fig. 11. The control problem is to select an appropriate control strategy for the switches in the front-end converter in order to achieve the dynamic and steady-state speed response requirements for the drive. Recalling from the case of dc motor speed control discussed in Section 2.1, the response requirements may be put in the following form:

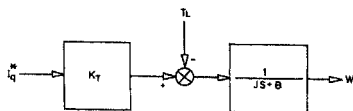


FIG. 10. Block diagram model of the current-fed BLDC motor drive. The system is linear and first order between  $I_q^*$  and  $\omega$ .

**Table II**  
**Switch inputs for constant current control**

Sector	$i_d > 0?$	$i_q > I_q^*?$	Switch inputs		
			A	B	C
$0^\circ < \omega t < 60^\circ$	0	0	1	1	0
	0	1	1	0	1
	1	0	0	1	0
	1	1	0	0	1
$60^\circ < \omega t < 120^\circ$	0	0	0	1	0
	0	1	1	0	0
	1	0	0	1	1
	1	1	1	0	1
$120^\circ < \omega t < 180^\circ$	0	0	0	1	1
	0	1	1	1	0
	1	0	0	0	1
	1	1	1	0	0
$180^\circ < \omega t < 240^\circ$	0	0	0	0	1
	0	1	0	1	0
	1	0	1	0	1
	1	1	1	1	0
$240^\circ < \omega t < 300^\circ$	0	0	1	0	1
	0	1	0	1	1
	1	0	1	0	0
	1	1	0	1	0
$300^\circ < \omega t < 360^\circ$	0	0	1	0	0
	0	1	0	0	1
	1	0	1	1	0
	1	1	0	1	1

Look-up table relating the input quantities, rotor MMF sector,  $d$  axis current ( $i_d > 0?$ ) and the  $q$  axis current ( $i_q > I_q^*?$ ) - directly into the necessary control action in terms of the inverter switch positions (A, B, C).

$$\sigma_q = (\omega - \omega^*) + \frac{d(\omega - \omega^*)}{dt} = 0. \quad (2.6.01)$$

The extra condition required to be satisfied for orthogonality between stator and rotor MMFs is that

$$\sigma_d = i_d = 0. \quad (2.6.02)$$

The value of  $\sigma_q$  at any instant (again recalling from Section 2.1) helps decide the need to accelerate or decelerate the motor. The need for acceleration or deceleration determines the polarity of  $i_q$  desired. From eqn (2.3.21) it is seen that increasing or

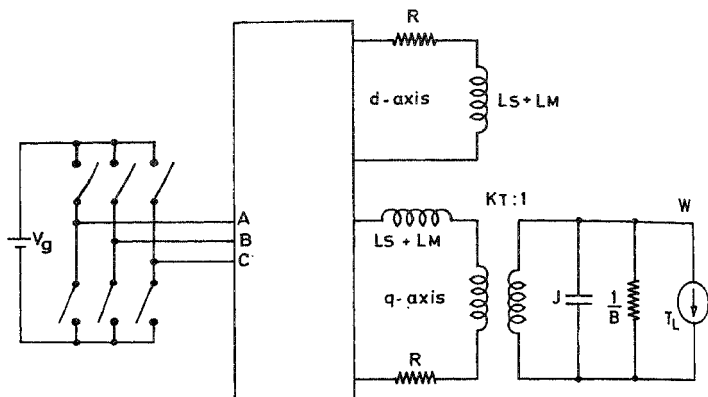


Fig. 11. The complete schematic of a BLDC motor drive. The electrical and the electromagnetic subsystems of the motor are given in the synchronously rotating ( $d$ ,  $q$ ) reference frame.

decreasing  $i_q$  eventually decelerates or accelerates the motor. The value of  $\sigma_d$  at any instant determines the corrective action desired in  $i_d$ . Given the values of  $\sigma_d$ ,  $\sigma_q$ , and the sector of the rotor MMF at any instant, a look-up table may be constructed to relate these conditions to the desired switch input (Table III). Table III is identical in its content to Table II used for current-controlled BLDC motor. The difference lies in the fact that positive  $i_q$  produces negative torque and *vice versa*.

### 3. Hardware and test results

#### 3.1 Current-controlled BLDC motor

The scheme explained in Section 2.5 was realized on a 1/2 hp BLDC motor. Recall that it is necessary to compute the direct axis current  $i_d$  and the quadrature axis current  $i_q$ .

Figure 12 shows the hardware to compute  $i_d$  and  $i_q$ . The Hall-effect current sensors generate analog signals proportional to the phase currents ( $i_A$ ,  $i_B$  and  $i_C$ ) of the motor. An incremental encoder drives the up/down counter to produce digital shaft position signal ( $\omega t$ ). The ABC- $\alpha$ ,  $\beta$  transformation block realizes eqn (2.3.08). It takes in analog phase current signals ( $i_A$ ,  $i_B$  and  $i_C$ ) to produce the two-phase current signals ( $i_a$  and  $i_b$ ). Two Eproms store the trigonometric functions  $\cos \omega t$  and  $\sin \omega t$ , and are addressed by the digital shaft position signal. Multiplying D/A converters realize eqns (2.3.16) and (2.3.17) to produce the analog direct and quadrature axes current signals.

Figure 13 shows the block diagram of the current-controlled BLDC motor. The two comparators sense the polarity of the error in the direct axis current  $i_d$  and the quadrature

**Table III**  
Switch inputs for sliding-mode speed

Sector	$\sigma_d > 0?$	$\sigma_q < \sigma_q^*?$	Switch inputs		
			A	B	C
$0^\circ < \omega t < 60^\circ$	0	0	1	1	0
	0	1	1	0	1
	1	0	0	1	0
	1	1	0	0	1
$60^\circ < \omega t < 120^\circ$	0	0	0	1	0
	0	1	1	0	0
	1	0	0	1	1
	1	1	1	0	1
$120^\circ < \omega t < 180^\circ$	0	0	0	1	1
	0	1	1	1	0
	1	0	0	0	1
	1	1	1	0	0
$180^\circ < \omega t < 240^\circ$	0	0	0	0	1
	0	1	0	1	0
	1	0	1	0	1
	1	1	1	1	0
$240^\circ < \omega t < 300^\circ$	0	0	1	0	1
	0	0	0	1	1
	1	0	1	0	0
	1	1	0	1	0
$300^\circ < \omega t < 360^\circ$	0	0	1	0	0
	0	1	0	0	1
	1	0	1	1	0
	1	1	0	1	1

Look-up table relating the input quantities, rotor MMF sector,  $d$  axis sliding line ( $\sigma_d > 0?$ ) and the  $q$  axis sliding line ( $\sigma_q > \sigma_q^*?$ ) directly into the necessary control action in terms of inverter switch positions (A, B, C).

axis current  $i_q$ . The sector sensor is realized with an Eprom. It senses the  $60^\circ$  wide sector in which the rotor MMF is located at any instant. From these inputs the look-up table selects the switch input for the three-phase input switches (Table II).

Figure 14a shows the phase currents  $i_A$  and  $i_B$ , and 14b currents  $i_\alpha$  and  $i_\beta$ . Figure 15 shows the stator MMF in the stationary frame of reference ( $i_\alpha$  vs  $i_\beta$ ). It is seen constant in magnitude and rotating in space at synchronous frequency.

Under current control the overall system ( $i_q$  vs  $\omega$ ) is a first order system whose time constant is the same as the mechanical time constant (J/B) of the motor. Figure 16 shows the step change in  $i_q$  and the consequent response in speed. This test is useful in determining the motor parameters. The time constant of the speed response gives the mechanical time constant (J/B) of the motor. The slope of the speed response ( $d\omega/dt$ ) as

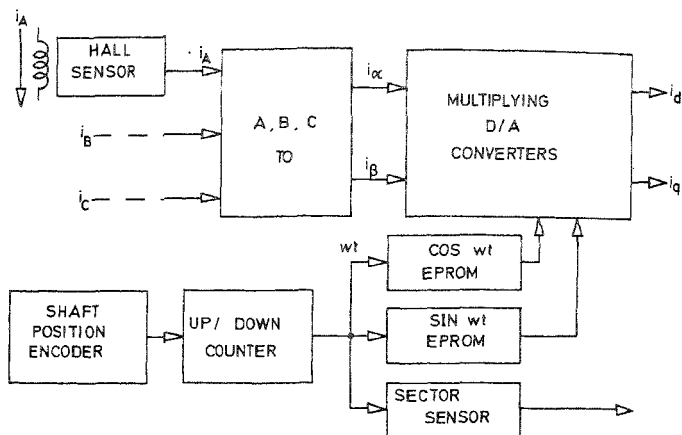


FIG. 12. Hardware for computing the direct axis and quadrature axis currents  $i_d$  and  $i_q$ .

the speed passes through zero speed is a measure of the load inertia ( $K_T i_q/J$ ). With a dynamometer load, the torque generated per ampere of  $i_q$  ( $K_T$ ) may be measured. From this test all the mechanical parameters of the motor may be experimentally determined.

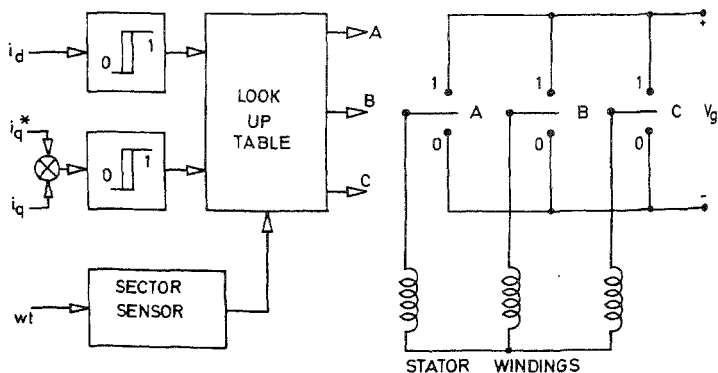
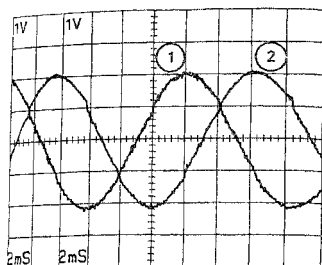
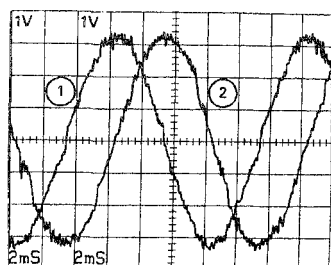


FIG. 13. Block diagram of the current-controlled BLDC motor drive. The switch inputs  $U_A$ ,  $U_B$ , and  $U_C$  are stored in the look-up table as a function of the errors in the direct and quadrature axes currents and the sector of the rotor MMF.



(a)  
Trace 1:  $i_A$ ; Trace 2:  $i_B$ ; Scale: 1 amp/div.



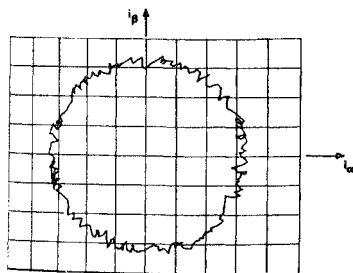
(b)  
Trace 1:  $i_\alpha$ ; Trace 2:  $i_\beta$ ; Scale: 1 amp/div.

FIG. 14. Current waveforms of a current-controlled BLDC motor. (a) shows the physical stator three-phase currents ( $i_A$  and  $i_B$ ). (b) shows the transformed two-phase currents  $i_\alpha$  and  $i_\beta$ .

As explained earlier in Section 2.5, an overall speed control loop may be designed around a current-controlled BLDC motor to meet speed control applications. Alternatively a direct sliding-mode speed control can be designed for such applications. In the following section the hardware and test results of such a controller are presented.

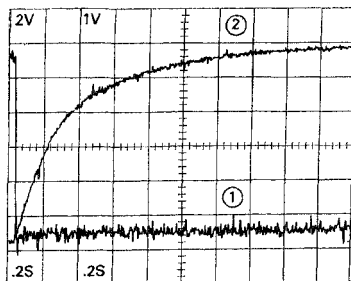
### 3.2 Sliding-mode speed controller

The sliding-mode speed controller given in Section 2.6 makes use of output speed and



X-Axis:  $i_\alpha$ ; 1 amp/div; Y-Axis:  $i_\beta$ ; 1 amp/div.

FIG. 15. The rotating stator MMF. The two-phase quantities  $i_\alpha$  and  $i_\beta$  enable viewing the stator MMF as  $i_\alpha$  vs  $i_\beta$  on the oscilloscope.



Trace 1:  $i_q$ ; 2 amps/div;  
Trace 2: W; 300 rpm/div.

FIG. 16. The response in speed of the current-controlled BLDC motor for step change in torque-producing current  $i_q$ . The electrical time constant of the motor being low, the response in current is almost instantaneous. The speed response is exponential with a time constant equal to the mechanical time constant of the motor.

speed derivative to directly measure  $\sigma_q$ . In a physical system the speed derivative is not directly accessible for measurement. Estimators may be used to obtain speed derivative. In practice the sliding line  $\sigma_q = 0$  as given in Section 2.6 can be modified with certain approximations as shown below.

Under the assumption that friction is low and that the load torque is constant or slowly varying, the mechanical system equation given by eqn (2.3.01) may be approximated as

$$K_T \dot{i}_q = J(d\omega/dt) \quad (3.2.01)$$

where  $\dot{i}_q$  is ac component of the torque producing quadrature axis current. The sliding line equation being a linear differential equation, one may represent the same in frequency domain as well.

$$\sigma_q(S) = (\omega - \omega^*) + \tau S(\omega - \omega^*). \quad (3.2.02)$$

From eqn (3.2.01), it is known that the quadrature axis current carries the speed derivative information. We may therefore modify the sliding line as

$$\sigma_q(S) = g(\omega - \omega^*) + \dot{i}_q(S). \quad (3.2.03)$$

Under sliding-mode control, since  $\sigma_q(S)$  is maintained to be zero, the resultant closed loop transfer function of the system is given by

$$\omega(S) = \frac{\omega^*(S)}{1 + S J/g K_T}. \quad (3.2.04)$$

Notice that unlike real sliding-mode control, now the response time is a function of the motor parameters and the speed gain  $g$ .

In eqn (3.2.03) the switching function  $\sigma_q$  is shown as the weighted sum of the speed error and the ac component of the quadrature axis current  $\dot{i}_q$ . In practice measurement of  $\dot{i}_q$  cannot be done instantaneously. It requires a high pass filter. The simplest realization of this filter is by means of an inverted pole. Equation (3.2.05) shows the practical switching function incorporating this practical necessity.

$$\sigma^*(S) = g \frac{1 + \omega_2/S}{1 + \omega_1/S} \omega - g \frac{\omega_1/S}{1 + \omega_1/S} \omega^* + \frac{1}{1 + \omega_1/S} \dot{i}_q(S) = 0. \quad (3.2.05)$$

It may be noted the speed is also measured with the same inverted pole as the current. In order not to lose the steady-state speed information an inverted zero has been added to the speed measurement. Equation (3.2.05) may be put in the following form for convenience.

$$\sigma^*(S) = g_1 \frac{1 + \tau_2 S}{1 + \tau_1 S} \omega - g_1 \frac{1}{1 + \tau_1 S} \omega^* + \frac{\tau_1 S}{1 + \tau_1 S} \dot{i}_q(S) = 0. \quad (3.2.06)$$

Under sliding mode control  $\sigma^*(S)$  is maintained to be zero. The closed loop response may therefore be computed from eqns (3.2.06) and (3.2.01) as follows

$$\omega(S) = \frac{\omega^*(S)}{1 + S/Q\omega_0 + S^2/\omega_0^2} \quad (3.2.07)$$

where

$$\begin{aligned} \omega_0^2 &= K_T g_1 / J \tau_1, \\ Q &= 1/\omega_0 \tau_2. \end{aligned} \quad (3.2.08)$$

The response as seen by eqn (3.2.07) is a second order response. Equation (3.2.08) gives the design criterion.  $\tau_1$  is the current filtering time constant and is chosen higher than the electrical time constant of the motor. The speed gain  $g_1$  is chosen to obtain the desired response time. The inverted zero frequency ( $1/\tau_2$ ) of speed measurement is chosen to obtain the desired damping. Figure 17 shows the block diagram of the controller. The switching functions  $\sigma_q$  and  $\sigma_d$  are realized as given in eqns (3.2.06) and (2.6.02) respectively. The switching decisions are stored in the look-up table as a function of sign ( $\sigma_q$ ), sign ( $\sigma_d$ ), and rotor position ( $\omega t$ ) (Table III).

In the circuit implementation of the sliding line, eqn (3.2.06) may be manipulated to obtain some more practical advantages. Equation (3.2.06) may be manipulated as

$$g_1 \frac{1 + \tau_2 S}{1 + \tau_1 S} \omega - g_1 \frac{1}{1 + \tau_1 S} \omega^* - \frac{1}{1 + \tau_1 S} i_q(S) = -i_q(S). \quad (3.2.09)$$

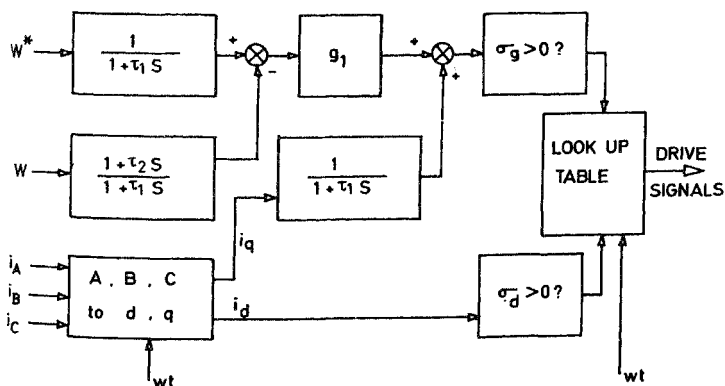


FIG. 17. The sliding-mode speed controller. Unlike the real sliding-mode control using the speed error and its derivative as the feedback variables, the modified sliding-mode controller uses the speed error and  $q$  axis current as the feedback variables. The state of the system ( $\sigma_d$  and  $\sigma_q$ ) at any instant and the sector in which the rotor MMF lies at any instant are used to look up into a table to decide the necessary control action.

In the case of current-controlled drive, the response in the current is almost instantaneous owing to the fact that the electrical time constant of the machine is quite low. Since we have chosen various filter time constants which are higher than the electrical time constant of the motor, the term  $i_q(S)$  on the RHS of eqn (3.2.09) may be replaced by  $I_q^*(S)$  giving rise to the following equation:

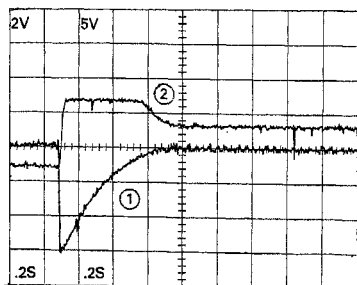
$$g_1 \frac{1}{1 + \tau_1 S} \omega^* - g_1 \frac{1 + \tau_2 S}{1 + \tau_1 S} \omega + \frac{1}{1 + \tau_1 S} i_q(S) = I_q^*(S). \quad (3.2.10)$$

Equation (3.2.10) is in such a form as to be added on conveniently to a current-controlled BLDC motor. Another added advantage is that overcurrent protection can be simply added by incorporating limits on this current reference signal  $I_q^*(S)$ .

Figures 18 and 19 show the response in speed error, and  $i_q$  for step speed reversal for two different compensator designs.

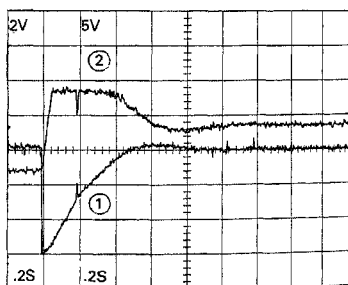
### 3.3 Some more practical aspects

From performance point of view the BLDC motor is seen to equal the dc motor drive. The electronic hardware is more complex because the reconstruction of the rotating reference frame currents  $i_d$  and  $i_q$  calls for position sensor of good resolution, multipliers, etc. With digital memory chips and D/A converters, the multipliers can be realized inexpensively. The position sensor is still one of the high-cost components of the system.



Trace 1: Speed error; 600 rpm/div; Trace 2: Current  $i_q$ ; 5 amps/div; Response: Second order;  $Q = 0.61$ ;  $\omega = 20.6$  rad/s.

FIG. 18. The response to step speed reversal command of a BLDC motor with sliding-mode controller. The controller design in this case results in an overdamped second order response.



Trace 1: Speed error; 600 rpm/div; Trace 2: Current  $i_q$ ; 5 amps/div; Response: Second order;  $Q = 1.2$ ;  $\omega = 10.8$  rad/s.

FIG. 19. The response to step speed reversal command of a BLDC motor with sliding-mode controller. The controller design in this case results in an underdamped second order response.

In this section some simplifications in the hardware for certain applications are outlined. Possible solution to overcome the disadvantages incurred owing to the above simplifications is identified in the design of the motor.

From Section 2.3, we may write the relationship between  $d$ - $q$  axis currents and the phase currents as below:

$$\begin{bmatrix} i_d \\ i_q \end{bmatrix} = \begin{bmatrix} -\cos \omega t & \sin \omega t \\ -\sin \omega t & -\cos \omega t \end{bmatrix} \begin{bmatrix} -\sqrt{3}/2 & \sqrt{3}/2 & 0 \\ -1/2 & -1/2 & 1 \end{bmatrix} \begin{bmatrix} i_A \\ i_B \\ i_C \end{bmatrix} \quad (3.3.01)$$

When we desire sinusoidal currents in the windings, the above transformations have to be realized with good accuracy of the trigonometric terms involved in eqn (3.3.01). Granting that non-sinusoidal phase currents are tolerable, the trigonometric terms in the above transformations may be replaced by the average of their end values in each of the  $60^\circ$  wide sectors of the rotor MMF position. For example, considering  $(0 < \omega t < 60^\circ)$  sector, the end values of the currents  $i_d$  and  $i_q$  are given by the following equations.

$$\begin{bmatrix} i_d \\ i_q \end{bmatrix}_{\omega=0} = \begin{bmatrix} -1 & 0 \\ 0 & -1 \end{bmatrix} \begin{bmatrix} -\sqrt{3}/2 & \sqrt{3}/2 & 0 \\ -1/2 & -1/2 & 1 \end{bmatrix} \begin{bmatrix} i_A \\ i_B \\ i_C \end{bmatrix}, \quad (3.3.02)$$

$$\begin{bmatrix} i_d \\ i_q \end{bmatrix}_{\omega=60^\circ} = \begin{bmatrix} -1/2 & +\sqrt{3}/2 \\ -\sqrt{3}/2 & -1/2 \end{bmatrix} \begin{bmatrix} -\sqrt{3}/2 & \sqrt{3}/2 & 0 \\ -1/2 & -1/2 & 1 \end{bmatrix} \begin{bmatrix} i_A \\ i_B \\ i_C \end{bmatrix}. \quad (3.3.03)$$

Taking the average of eqns (3.3.02) and (3.3.03), we may write for the sector  $0 < \omega t < 60^\circ$

$$\begin{bmatrix} i_d \\ i_q \end{bmatrix}_{(0 < \omega t < 60^\circ)} = \begin{bmatrix} \frac{3\sqrt{3}}{4} i_A \\ (3/4) (i_B - i_C) \end{bmatrix} \quad (3.3.04)$$

Further simplification is possible since under sliding control  $i_d$  is zero. Then it follows that

$$\begin{bmatrix} d \\ q \end{bmatrix}_{(0 < \omega t < 60^\circ)} = \begin{bmatrix} \frac{3\sqrt{3}}{4} i_A \\ (3/2) i_B \end{bmatrix} \quad (3.3.05)$$

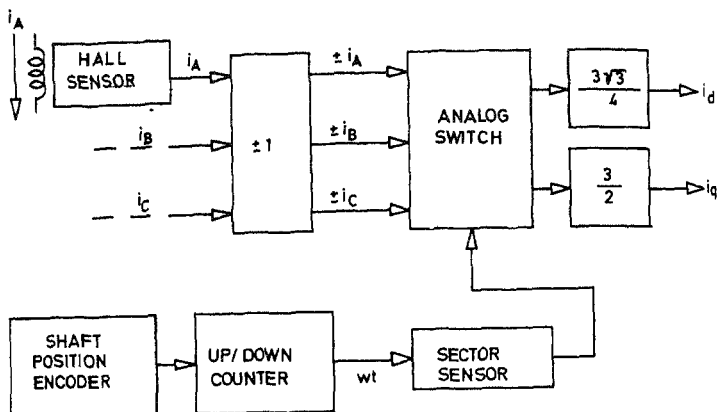
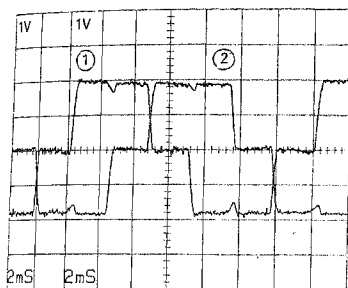


FIG. 20. Hardware for approximate computation of the direct and quadrature axes currents according to Table IV.

Table IV  
Approximations of  $I_d$  and  $I_q$

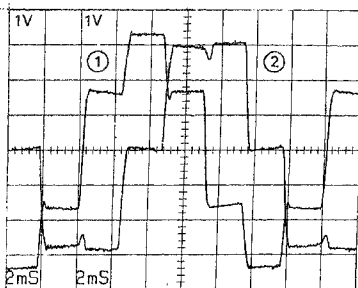
Sector	$I_d$	$I_q$
$0^\circ < \omega t < 60^\circ$	$\frac{+3\sqrt{3}}{4} I_A$	$\frac{3}{2} I_B$
$60^\circ < \omega t < 120^\circ$	$\frac{-3\sqrt{3}}{4} I_C$	$\frac{3}{2} I_B$
$120^\circ < \omega t < 180^\circ$	$\frac{+3\sqrt{3}}{4} I_B$	$\frac{3}{2} I_C$
$180^\circ < \omega t < 240^\circ$	$\frac{-3\sqrt{3}}{4} I_A$	$\frac{3}{2} I_C$
$240^\circ < \omega t < 300^\circ$	$\frac{+3\sqrt{3}}{4} I_C$	$\frac{3}{2} I_A$
$300^\circ < \omega t < 360^\circ$	$\frac{-3\sqrt{3}}{4} I_B$	$\frac{3}{2} I_A$

Approximate relationship between  $d$ ,  $q$  axes currents and the three-phase currents. From this relationship  $i_d$  and  $i_q$  may be approximately pieced together from the phase currents with the use of only sector sensors and analog switches instead of position sensors and multipliers.



Trace 1:  $i_a$ ; 1 amp/div; Trace 2:  $i_b$ ; 1 amp/div.

FIG. 21. Phase-current waveforms when the approximations given in Table IV are used to measure  $i_d$  and  $i_q$ . These approximations lead to the well-known quasi-square wave control of the motor.



Trace 1:  $i_\alpha$ ; 1 amp/div; Trace 2:  $i_\beta$ ; 1 amp/div.

FIG. 22. The equivalent two-phase ( $i_\alpha$  and  $i_\beta$ ) currents when the approximations given in Table IV used to measure  $i_d$  and  $i_q$ . The two-phase currents ( $i_\alpha$  and  $i_\beta$ ) are familiar six-step wave forms.

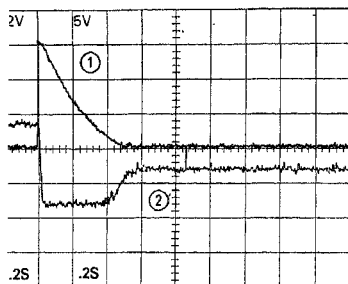
Using the above idea we may piece together the currents  $i_d$  and  $i_q$  from the appropriate phase currents in each of the sectors. The piece-wise relationship between the currents  $i_d$  and  $i_q$  and the phase currents is given in Table IV.

Figure 20 shows the block diagram of the hardware needed to compute  $i_d$  and  $i_q$  approximately according to eqn (3.3.05). Comparing with fig. 12, we see that reconstructing the currents  $i_d$  and  $i_q$  using Table IV requires only a sector sensor (much less expensive than a high resolution position sensor) and analog switches instead of multipliers. Considerable simplification is possible by following the above method of generating  $i_d$  and  $i_q$ . For good many applications the difference in performance because of the above changes is imperceptible. Figure 21 shows the phase currents under such a control, fig. 22 currents  $i_\alpha$  and  $i_\beta$ , and fig. 23 the response in speed error and  $i_q$  for step reversal in speed command under such a control.

It may be seen that the phase current waveforms are quasi-square wave. As a result the generated torque will be pulsating causing difficulties at low speeds. This problem exists only if the motor has a sinusoidal distribution of flux. However, if the motor can be built with trapezoidal distribution of flux, the low-speed performance can be considerably improved.

#### 4. Conclusion

The sliding-mode control approach had been applied to the speed control of BLDC motor. The control strategy is very simple to realize. True dc motor operation of the synchronous motor is achieved resulting in self starting and stable operation at all speeds. The compensator design is simple and provides overcurrent protection too. Experimental results verify the design procedure.



Trace 1: Speed error; 600 rpm/div; Trace 2: Current  $i_q$ ; 5 amps/div; Response: Second order;  $Q = 0.61$ ;  $\omega = 20.6$  rad-s.

FIG. 23. The response to step speed reversal command when piecewise approximation to evaluate  $i_d$  and  $i_q$  is used. The response is practically indistinguishable from the one given in fig. 18, where the more accurate trigonometric transformations are used to evaluate  $i_d$  and  $i_q$ .

The BLDC motor drive performance equals the dc motor drive. In view of the robustness of the motor, the BLDC motor provides an attractive option for variable speed applications. With high speed switches the motor may be designed with higher number of poles for operation at higher synchronous frequency resulting in higher power density for the motor. With trapezoidal flux distribution further simplification in the electronic hardware is possible.

### Acknowledgement

This work was supported in part by the General Dynamics Corporation, Fort Worth, Texas and by Caltech's program in Advanced Technologies, sponsored by Aerojet General, General Motors, GTE and TRW.

### References

- BOSE, B.K. (ed) *Adjustable speed ac drive systems*, IEEE Press, New York, 1981.
- BLASCHKE, F. The principle of field orientation as applied to the new TRANSVEKTOR closed loop control system for rotating-field machines, *Siemens Rev.*, 1972, 39, 217.
- UTKIN, V. I. *Sliding modes and their application in variable structure systems*, Mir, Moscow, 1978.
- VENKATARAMANAN, R. *Sliding mode control of power converters*, Ph.D. Thesis, Caltech, Pasadena, 1986.